

## Strain derivatives of $T_c$ in $\text{HgBa}_2\text{CuO}_{4+\delta}$ : The $\text{CuO}_2$ plane alone is not enough

Shibing Wang,<sup>1,2,\*</sup> Jianbo Zhang,<sup>3</sup> Jinyuan Yan,<sup>4</sup> Xiao-Jia Chen,<sup>5,6</sup> Viktor Struzhkin,<sup>5</sup> Wojciech Tabis,<sup>7,8</sup> Neven Barišić,<sup>7,9</sup> Mun K. Chan,<sup>7</sup> Chelsey Dorow,<sup>7</sup> Xudong Zhao,<sup>7,10</sup> Martin Greven,<sup>7</sup> Wendy L. Mao,<sup>1,11</sup> and Ted Geballe<sup>12</sup>

<sup>1</sup>Department of Geological and Environmental Sciences, Stanford University, Stanford, California 94305, USA

<sup>2</sup>SIMES, SLAC National Accelerator Laboratory, Menlo Park, California 94025, USA

<sup>3</sup>Department of Physics, South China University of Technology, Guangzhou 510640, China

<sup>4</sup>Advanced Light Source, Lawrence Berkeley National Laboratory, Berkeley, California 94720, and Earth and Planetary Sciences, University of California, Santa Cruz, California 95064, USA

<sup>5</sup>Geophysical Laboratory, Carnegie Institution of Washington, Washington, DC 20015, USA

<sup>6</sup>Center for High Pressure Science and Technology Advanced Research, Shanghai 201203, China

<sup>7</sup>School of Physics and Astronomy, University of Minnesota, Minneapolis, Minnesota 55455, USA

<sup>8</sup>AGH University of Science and Technology, Faculty of Physics and Applied Computer Science, 30-059 Krakow, Poland

<sup>9</sup>Service de Physique de l'Etat Condensé CEA-DSM-IRAMIS, 91198 Gif-sur-Yvette, France

<sup>10</sup>State Key Lab of Inorganic Synthesis and Preparative Chemistry, Jilin University, Changchun 130012, China

<sup>11</sup>Photon Science, SLAC National Accelerator Laboratory, Menlo Park, California 94025, USA

<sup>12</sup>Department of Applied Physics and Geballe Laboratory for Advanced Materials, Stanford University, Stanford, California 94305, USA

(Received 1 October 2013; revised manuscript received 7 January 2014; published 29 January 2014)

The strain derivatives of  $T_c$  along the  $a$  and  $c$  axes have been determined for  $\text{HgBa}_2\text{CuO}_{4+\delta}$  (Hg1201), the simplest monolayer cuprate with the highest  $T_c$  of all monolayer cuprates ( $T_c = 97$  K at optimal doping). The underdoped compound with the initial  $T_c$  of 65 K has been studied as a function of pressure up to 20 GPa by magnetic susceptibility and x-ray diffraction. The observed linear increase in  $T_c$  with pressure is the same as previously found for the optimally doped compound. The above results have enabled an investigation of the origins of the significantly different  $T_c$  values of optimally doped Hg1201 and the well-studied compound  $\text{La}_{2-x}\text{Sr}_x\text{CuO}_4$  (LSCO), which has a maximal  $T_c$  of 40 K, or only 40% of that of Hg1201. Hg1201 can have almost identical  $\text{CuO}_6$  octahedra as LSCO if specifically strained. When the apical and in-plane  $\text{CuO}_2$  distances are the same for the two compounds, a large discrepancy in their  $T_c$  remains. Differences in crystal structures and interactions involving the Hg-O charge reservoir layers of Hg1201 may be responsible for the different  $T_c$  values exhibited by the two compounds.

DOI: [10.1103/PhysRevB.89.024515](https://doi.org/10.1103/PhysRevB.89.024515)

PACS number(s): 74.72.-h, 62.20.D-, 62.50.-p, 74.62.Fj

### I. INTRODUCTION

More than two decades after the discovery of high-temperature superconductors with superconducting transition temperature ( $T_c$ ) above the liquid nitrogen boiling point, the mechanisms leading to such extraordinarily high  $T_c$  values remain unclear. Correlated electrons within the copper-oxygen planes form Cooper pairs.  $T_c$  is a function of cation or oxygen doping. It rises to a maximum at optimal doping and then falls in a “dome”-like trajectory [1,2]. When subject to pressure,  $T_c$  of some optimally doped compounds increases at a rate of 1–2 K/GPa before saturating at a certain pressure. Among these cuprates is the mercury family, which are model systems with copper-oxygen planes sandwiched by mercury oxygen planes:  $\text{HgBa}_2\text{Ca}_{n-1}\text{Cu}_n\text{O}_{2n+2+\delta}$  ( $n = 1, 2, 3, \dots, 9$ ) [3,4]. The trilayer compound ( $n = 3$ ) holds the record  $T_c$  of 164 K when compressed to 30 GPa [3].

Strain effects on the  $T_c$  of the cuprate superconductors provide important information to help guide the development of adequate theoretical models and, potentially, for the design of materials with higher values of  $T_c$ . There have been a number of high-pressure studies on optimally doped Hg1201, investigating how lattice parameters, atomic positions, and  $T_c$  changes under both hydrostatic and uniaxial pressure [3,5–7]. The uniaxial  $dT_c/dP_l$  ( $l = a, b, c$ ) has been found

from the Ehrenfest relationship  $dT_c/dP_l = \Delta\alpha_l V_m T_c / \Delta C_p$  using experimental values of the thermal expansion ( $\alpha_l$ ), heat capacity ( $\Delta C_p$ ), and molar volume ( $V_m$ ) [8]. The hydrostatic  $dT_c/dP$ , on the other hand, is directly determined from either susceptibility or transport measurements. These values are essentially the *stress* derivatives of  $T_c$ . To test current theories, the *strain* coefficients  $dT_c/(dl/l)$  are particularly useful. By obtaining the strain derivatives of  $T_c$  along the different crystallographic axes, we aim to establish that the large discrepancy in  $T_c$  between Hg1201 and  $\text{La}_{2-x}\text{Sr}_x\text{CuO}_4$  (LSCO) cannot be explained by interactions confined to the  $\text{CuO}_2$  planes alone.

In this article, we present the dependence of  $T_c$  and structure on pressure for underdoped single crystals of Hg1201 with an ambient  $T_c$  of 65 K measured up to 20 GPa in diamond anvil cells (DACs). We find that the rate of  $T_c$  increase agrees with that of optimally doped Hg1201 [3,5,9] for a wide pressure range. The effect of pressure, either uniaxial or hydrostatic, on  $T_c$  is linear, i.e.,  $dT_c/dP_l$  and  $dT_c/dP$  (hydrostatic) are constant, up to 10 GPa for both underdoped and optimally doped Hg1201, which suggests that pressure is tuning interactions that are independent of the carrier density [10].

### II. EXPERIMENTAL METHODS

The samples measured in the present experiment were grown with an encapsulation method and subsequently annealed to yield a  $T_c$  of 65 K [11,12]. For the  $T_c$  measurement, a

\*shibingw@stanford.edu

$120 \times 80 \times 30 \mu\text{m}^3$  single crystal was loaded into a Mao-Bell DAC made from hardened Be-Cu alloy. A nonmagnetic Ni-Cr alloy gasket preindented to  $35 \mu\text{m}$  thick with a  $250\text{-}\mu\text{m}$ -diameter hole served as the sample chamber. Daphne 7373 was loaded into the gasket hole as a pressure medium. An ac circuit consisted of a signal coil around the diamonds, a compensating coil nearby, and a larger pick-up coil was used to measure susceptibility, as detailed previously [13–15]. The single crystal was visually inspected with an optical microscope, and remained intact throughout the experiment. The high-pressure angle-dispersive synchrotron x-ray diffraction (XRD) experiment was conducted at Beamline 12.2.2 of the Advanced Light Source (ALS), Lawrence Berkeley National Laboratory (LBNL), with an incident x-ray wavelength of  $0.6199 \text{ \AA}$ . A sample from the same mother crystal was ground into a powder in an agate motor and was loaded to a symmetric DAC with a stainless steel gasket in a hole with  $150 \mu\text{m}$  diameter; the diamond culet was  $300 \mu\text{m}$ . Ne gas was loaded into the sample chamber as the pressure medium with the GSECars gas loading system at the Advanced Photon Source (APS), Argonne National Laboratory (ANL) [16]. Good hydrostaticity was maintained to the highest pressures measured. Two-dimensional (2D) diffraction patterns from a MAR345 image plate were integrated using FIT2D [17]. Rietveld refinement was performed on the powder diffraction pattern [18]. In both measurements, small ruby chips placed in the DACs were used for pressure calibration [19].

### III. RESULTS AND DISCUSSION

Figure 1 shows the in-phase component of the modulated signal versus temperature for underdoped Hg1201. For each pressure run, the signal was measured during both cooling and warming cycles.  $T_c$  is taken as the intersection of the extrapolated linear rise with the base line [13]. Pressures were measured 10–15 K above the transition temperature. When the sample was warmed up to 120 K, pressure was increased, and after 30 min of relaxation,  $T_c$  was measured at the new pressure. The  $T_c$  of underdoped Hg1201 increased from 65 K at ambient pressure to 84 K at 17 GPa. Upon reducing the pressure back to ambient [20], the high  $T_c$  (84 K) was not retained, and the signal amplitude was not recovered.

The inset of Fig. 1 shows that the amplitude of the signal increases with increasing pressure before decreasing significantly at 12 GPa. Previous resistivity measurements on optimally doped Hg1201 suggest that defects are introduced at high quasi-hydrostatic pressure, causing irreversible degradation of the sample above 10 GPa [3].

Figure 2 shows that  $T_c$  increases linearly with applied pressure up to  $\sim 10$  GPa. The increase of  $T_c$  compared to ambient pressure ( $\Delta T_c$ ) is also plotted to compare with the  $\Delta T_c$  of optimally doped Hg1201 measured resistively [3]. Two observations can be made: First, the linearity range of  $dT_c/dP$  extends up to  $\sim 10$  GPa in Hg1201, approximately the same pressure above which the susceptibility measurements indicate sample degradation (Fig. 1); second, the  $\Delta T_c$  response of Hg1201 to pressure is almost identical for underdoped and optimally doped samples. Such an agreement of underdoped and optimally doped Hg1201 was previously observed only up to 1.7 GPa [21].

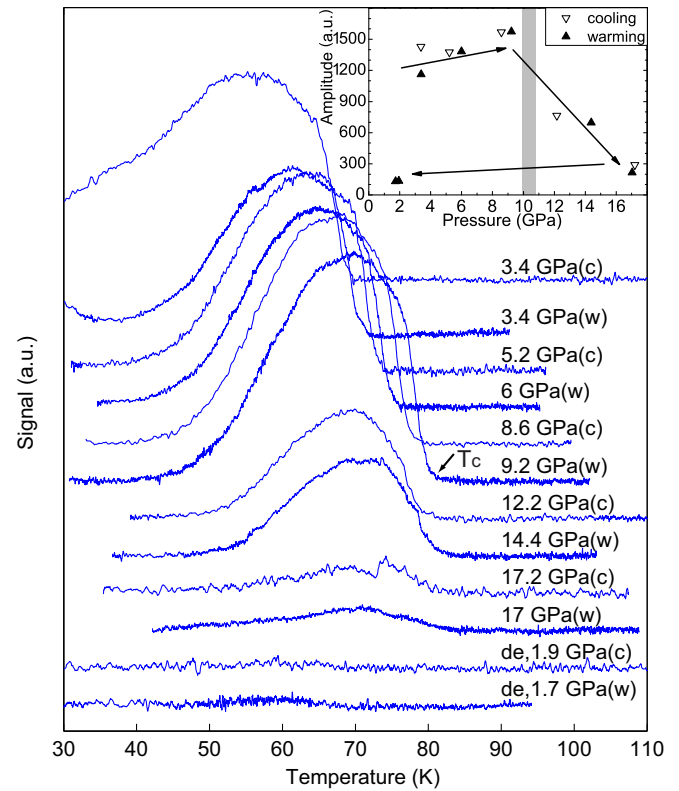


FIG. 1. (Color online) In-phase component of susceptibility signal measured during both cooling and warming cycles at each pressure run. The run started with 3.4 GPa and pressure was increased to 17 GPa. Pressure was then immediately released to 1.9 GPa. “de” is short for decompression. Inset: Strength of the susceptibility signal as a function of pressure. Arrows indicate the measurement sequence. Gray bar indicates the pressure where sample starts to degrade.

Structural information for Hg1201 is summarized in Fig. 3. The pressure dependence of the (003), (110) and (200) Bragg

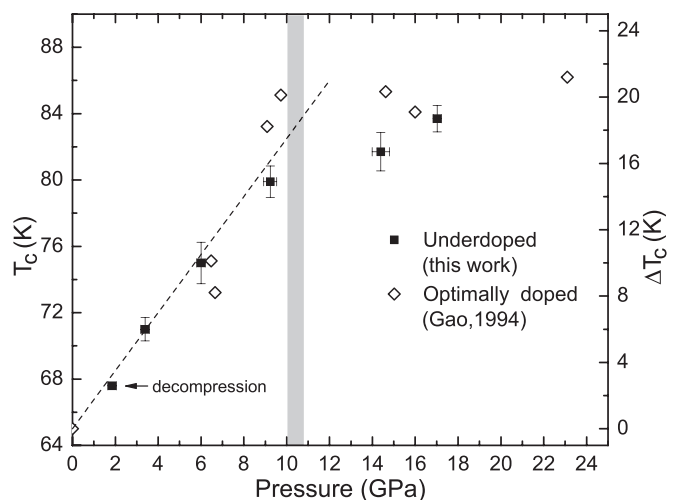


FIG. 2.  $T_c$  and  $\Delta T_c$  vs pressure. Filled squares:  $T_c$  of the underdoped sample measured in the warming cycle. Open diamonds:  $\Delta T_c$  of the optimally doped sample [3]. The dashed line corresponds to  $dT_c/dP = 1.75 \text{ K/GPa}$  [9]. The gray bar indicates the pressure where the sample starts to degrade.

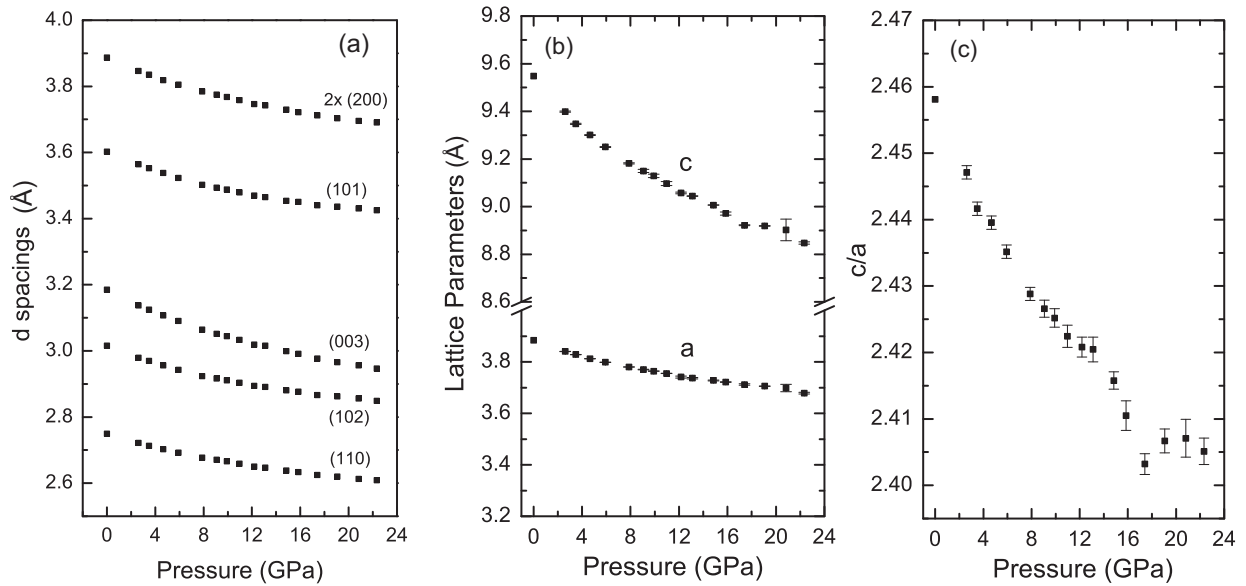


FIG. 3. (a) The  $d$  spacings for the (110), (102), (003), (101), and (200) Bragg reflections as a function of pressure for underdoped Hg1201. (b) Lattice parameters and (c)  $c/a$  ratio as a function of pressure.

peak positions indicates that lattice parameter  $c$  decreases at a faster rate than  $a$ , consistent with a previous report for optimally doped Hg1201 [6]. The lattice parameters and volume were fit to a third-order Birch-Murnaghan equation with  $K'_0 = 4$  [23]. We obtain axes and volume bulk moduli  $Ka_0$ ,  $Kc_0$ , and  $KV_0$  of 83.6, 54.3, and 69.1 GPa, respectively; the first two correspond to the  $a$  and  $c$  axial compressibilities  $\kappa_a, \kappa_c$  [ $\kappa_{a,c} = 1/(3Ka_{0,c0})$ ] of  $3.99 \times 10^{-3}$  and  $6.13 \times 10^{-3}$  GPa<sup>-1</sup> at ambient pressure. These values agree well with those for optimal doping [5,6,22], indicating that to first order, we can use these structure and elastic constants for Hg1201 for both the underdoped and optimally doped cases. Compressibilities at 7 and 11 GPa are given in Table I. Due to peak broadening and weaker signals, the refinement at higher pressure is less accurate. The  $c/a$  ratio decreases approximately linearly up to  $\sim 10$  GPa and exhibits a more complicated dependence at higher pressures [Fig. 3(c)]. The anomalous region coincides with where the susceptibility signal decreases significantly (Fig. 1), and it reflects the intrinsic sample change above 10–12 GPa. The identical  $T_c$  responses to external pressure and similar  $a$  and  $c$  compressibilities for underdoped and optimally doped Hg1201 suggest that the rate at which the charge reservoir layer is brought toward the CuO<sub>2</sub> plane correlates with the rate of  $T_c$  increase regardless of the initial charge-carrier density.

We now focus on the strain derivative  $dT_c/(dl/l)$  for Hg1201. A series of uniaxial pressure and hydrostatic pressure experiments have been previously conducted on several cuprates, e.g., YBa<sub>2</sub>Cu<sub>3</sub>O<sub>7- $\delta$</sub> , Tl<sub>2</sub>Ba<sub>2</sub>CuO<sub>6+ $\delta$</sub> , and Hg1201 [7,24–26].  $dT_c/dP_l$  ( $l = a, b,$  or  $c$ ) was obtained from the Ehrenfest relation. This is thermodynamically accurate for mean-field transitions, but it introduces some uncertainty in the Hg1201 case, where the  $C_p$  anomaly spreads over two decades in temperature with no obvious discontinuous jump [27]. With the compressibilities of  $a$  and  $c$  from our hydrostatic pressure XRD experiment, and making the reasonable assumption that

Poisson's ratio  $-\frac{dc/c}{da/a} = -\frac{db/b}{da/a} = 0.2$  [28], we can obtain the relevant terms in the strain-stress compliance matrix of a tetragonal system (see the Appendix for details). We use the widely accepted (and verified in the present work) value  $dT_c/dP = 1.75$  K/GPa [8,9] and the best available  $dT_c/dP_a = 2.3$  K/GPa or  $dT_c/dP_c = -3.6$  K/GPa from a uniaxial pressure experiment [7]. The calculated values of  $dT_c/(dc/c)$  and  $dT_c/(da/a)$  at different pressure are shown in Table I. Even though  $dT_c/dP_c$  is larger in magnitude than  $dT_c/dP_a$ , the actual  $T_c$  response to the  $c$ -axis strain is smaller. The ratio of the magnitude of  $dT_c/da$  to  $dT_c/dc$  lies between

TABLE I. Geometry of the CuO<sub>6</sub> octahedra for Hg1201 and LSCO at different pressure and temperature conditions, and strain derivatives of  $T_c$  for Hg1201. Lattice parameters and compressibilities are from this study. Values of Cu-O<sub>apical</sub> are extrapolated from a neutron scattering study [5].  $T_c$  for optimally doped Hg1201 is from [3]; its buckling angle is extrapolated from [5]. The structure of LSCO is from [29], and its  $T_c$  is from [30]. The uncertainty of the strain derivatives of  $T_c$  comes from the slight disagreement of the uniaxial and hydrostatic stress derivatives and the choice of Poisson's ratio.

Condition	Hg1201 ambient	Hg1201 7 GPa	Hg1201 11 GPa	La <sub>1.85</sub> Sr <sub>0.15</sub> CuO <sub>4</sub> 60 K
$a$ (Å)	3.885	3.78	3.754	3.78
$c$ (Å)	9.549	9.205	9.089	6.59
Cu-O <sub>apical</sub> (Å)	2.789	2.552	2.417	2.41
Buckling (deg)	180	180	180	175.5
$T_c$ (K)	97	108	116	40
$\kappa_a$ (10 <sup>-3</sup> /GPa)	3.99	3.01	2.66	
$\kappa_c$ (10 <sup>-3</sup> /GPa)	6.14	4.11	3.49	
$dT_c/(da/a)$ (K)	-433(50)	-565(60)	-638(70)	
$dT_c/(dc/c)$ (K)	278(60)	402(80)	469(100)	

3.8 and 4.5, and  $dT_c/(da/a)$  to  $dT_c/(dc/c)$  is 1.5–1.8 in Hg1201 at ambient pressure.

For uniaxial pressure along the  $c$  axis, the compression is accompanied by the expansion of the other two axes, i.e.,  $dT_c/dP_c = \frac{\partial T_c}{\partial c} \frac{\partial c}{\partial P_c} + 2 \frac{\partial T_c}{\partial a} \frac{\partial a}{\partial P_c}$ : both terms are negative with applied uniaxial pressure  $P_c$ . The large negative value of  $dT_c/dP_c$  is from the combination of  $c$ -axis compression and  $ab$ -plane expansion. The  $T_c$  derivatives of the strain, on the other hand, separate these effects, and give direct information on how  $T_c$  changes with a different axis independently.

Our calculation of  $dT_c/(dl/l)$  for Hg1201 provides the means for comparing the  $T_c$  values of different families of cuprate superconductors. Here we compare the single-layer optimally doped LSCO ( $T_c = 40$  K) with Hg1201 ( $T_c = 97$  K). With hydrostatic pressure,  $T_{c,\max}$  of LSCO reaches 42 K at 4 GPa, whereas for Hg1201 it reaches 118 K at 23 GPa. Hg1201 and LSCO differ in a number of ways: LSCO has a body-centered structure and transforms to orthorhombic at low temperature which buckles the  $\text{CuO}_2$  planes [29], while Hg1201 has a simple tetragonal structure; the former has a shorter interlayer distance and apical oxygen distance and smaller  $\text{CuO}_2$  plane area; in addition, differences in disorder have been noted [34]. We aim to discern what the contributing factors are in the following discussion.

The lattice parameters and sizes of the  $\text{CuO}_6$  octahedra of Hg1201 at different pressures are shown in Table I: at 7 GPa, the  $ab$  plane of Hg1201 is of the same size as that of LSCO, while the apical oxygen distance is still 0.14 Å larger than that of the latter. With  $dT_c/(dc/c) = 402$  K (at  $P = 7$  GPa),  $T_c$  is only reduced to 86 K, far above the  $T_{c,\max}$  of optimally doped LSCO (40 K) [29,30]. If we further increase pressure to 11 GPa, the apical oxygen distance of Hg1201 matches that of LSCO. Then, expanding  $a$  by 0.026 Å from 3.754 to 3.78 Å (Table I) for Hg1201 will only reduce  $T_c$  by 4 K. While we are aware of the complexity of the Cu-O-Cu buckling angle of Hg1201 [31], the difference in buckling angle between Hg1201 and LSCO would not account for much: high pressure reduces the buckling angle of LSCO to nearly  $180^\circ$  and makes the structure tetragonal [32], but it only increases its  $T_c$  by a few Kelvin [33].  $A$ -site (La site) disorder in LSCO influences  $T_c$  through the hybridization between the orbitals of the apical  $\text{O}(2p_z)$  and  $\text{Cu}(3d_{x^2-y^2-3z^2})$  [34]. However, for the oxygen doped  $\text{La}_2\text{CuO}_{4+\delta}$ , where  $A$ -site disorder does not exist and additional oxygen is confined to interstitial sites [35], its  $T_c$  only rises to 42 K [36].

After adjusting the geometrical difference in the  $\text{CuO}_6$  octahedra of Hg1201 and LSCO, there still remains a 44 K difference in  $T_c$  values between the two cuprates. A recent theoretical model which explicitly includes the Cu  $d_{x^2-y^2}$ ,  $d_{z^2}$ , and  $4s$  orbitals qualitatively predicts correctly the larger  $T_c$  value of Hg1201 [37] and the sign of  $dT_c/dP_l$  and  $dT_c/dP$  [38]. The model attributes the low  $T_c$  of LSCO to the compound's body-centered-tetragonal structure, in close proximity to apical oxygen atoms of neighboring  $\text{CuO}_2$  layers, which causes an elevation of the  $d_{z^2}$  Wannier orbital [39].

However, the effect of the Hg-O layers seems to be more than merely separating the  $\text{CuO}_6$  octahedra, as they exhibit a high degree of polarizability and hence serve to screen long-range Coulomb interactions in the quintessential  $\text{CuO}_2$  sheets [40,41]. We note that the above considerations have

focused on average bond distances and bond angles. There exists ample evidence from local bulk probes that the cuprates exhibit significant compound-specific local deviations from the average crystal structure [42,43], and that the charge distributions in both LSCO [44] and Hg1201 [45] vary on the nanoscale. Based on modeling the disorder in the interstitial layers, it was concluded that the hole mean free path and the screening of the Coulomb repulsion in Hg1201 are substantially larger than in LSCO, hence contributing to the higher  $T_c$  [40]. To fully account for the differences between the two compounds, further consideration of the screening of electronic inhomogeneity inherent to the  $\text{CuO}_2$  planes may be necessary. In this context, it is important to note that the Hg-O layers in Hg1201 may have metallic character that could be enhanced at elevated pressure [46,47].

#### IV. CONCLUDING REMARKS

In summary, through high-pressure susceptibility and structure measurement of underdoped Hg1201, we obtained the hydrostatic  $dT_c/dP$  and relevant elastic constants of the compound. Together with previously reported  $dT_c/dP_l$ , we have determined  $dT_c/(dl/l)$  for Hg1201. Our results show that  $T_c$  is more sensitive to the strain change along the  $a$  axis than the  $c$  axis. A comparison of strained Hg1201 to optimally doped LSCO indicates that to account for the large  $T_c$  discrepancy, theories need to consider factors beyond the geometry of the  $\text{CuO}_6$  octahedra.

#### ACKNOWLEDGMENTS

The authors are grateful for discussion with W. Nix, S. Raghu, D. Scalapino, and G. Yu. The authors thank S. Tkachev for help with gas loading at the Advanced Photon Source. S.W., Z.J.B., X.J.C., V.S., and W.L.M. are supported by EFree, an Energy Frontier Research Center funded by the U.S. Department of Energy (DOE), Office of Science, Office of Basic Energy Sciences (BES) under Contract No. DE-SG0001057. Travel to facilities is supported by Stanford Institute for Materials and Energy Science (Contract No. DE-AC02-76SF00515). The work at the University of Minnesota was supported by DOE-BES under Contract No. DE-SC0006858. N.B. acknowledges support through a Marie Curie Fellowship. A.L.S. is supported by DOE-BES under Contract No. DE-AC02-05CH11231.

#### APPENDIX

This Appendix describes the derivation of the strain derivative of  $T_c$  ( $dT_c/d\epsilon$ ) from the experimentally measured stress derivative ( $dT_c/d\sigma$ ) in Hg1201 used in this study. The key is to construct the strain-stress compliance matrix. Some of the elastic constants were obtained in this high-pressure x-ray diffraction study. For some of the others, we made reasonable assumptions. We present the details of constructing the compliance matrix and converting  $dT_c/d\sigma$  to  $dT_c/d\epsilon$  of Hg1201 in the following subsections.

##### 1. Constructing the strain-stress compliance matrix

Hydrostatic high-pressure experiments fix the stress, and one measures the strain through x-ray diffraction (XRD).



Therefore, the compliance matrix shall be used. To start, we have

$$\epsilon_i = S_{ij}\sigma_j,$$

where we choose the crystal coordinates  $\epsilon_1 = da/a$ ,  $\epsilon_2 = db/b$ , and  $\epsilon_3 = dc/c$ . For a tetragonal crystal system,  $S_{i,j}$  is reduced to

$$\begin{pmatrix} \epsilon_1 \\ \epsilon_2 \\ \epsilon_3 \\ \epsilon_4 \\ \epsilon_5 \\ \epsilon_6 \end{pmatrix} = \begin{pmatrix} s_{11} & s_{12} & s_{13} & & & s_{16} \\ s_{12} & s_{11} & s_{13} & & & -s_{16} \\ s_{13} & s_{13} & s_{33} & & & \\ & & & s_{44} & & \\ & & & & s_{44} & \\ s_{16} & -s_{16} & & & & s_{66} \end{pmatrix} \begin{pmatrix} \sigma_1 \\ \sigma_2 \\ \sigma_3 \\ \sigma_4 \\ \sigma_5 \\ \sigma_6 \end{pmatrix}.$$

In hydrostatic compression with external pressure  $P$ , this becomes

$$\begin{pmatrix} \epsilon_1 \\ \epsilon_2 \\ \epsilon_3 \end{pmatrix} = \begin{pmatrix} s_{11} & s_{12} & s_{13} \\ s_{12} & s_{11} & s_{13} \\ s_{13} & s_{13} & s_{33} \end{pmatrix} \begin{pmatrix} -P \\ -P \\ -P \end{pmatrix},$$

which gives

$$\epsilon_1 = \epsilon_2 = -P(s_{11} + s_{12} + s_{13}), \quad (\text{A1})$$

$$\epsilon_3 = -P(2s_{13} + s_{33}). \quad (\text{A2})$$

With high-pressure XRD, the compressibilities  $\kappa_a = -\epsilon_1/P$  and  $\kappa_c = -\epsilon_3/P$  are known.

In  $c$ -axis uniaxial loading with  $P_c$ , we have

$$\begin{pmatrix} \epsilon_1 \\ \epsilon_2 \\ \epsilon_3 \end{pmatrix} = \begin{pmatrix} s_{11} & s_{12} & s_{13} \\ s_{12} & s_{11} & s_{13} \\ s_{13} & s_{13} & s_{33} \end{pmatrix} \begin{pmatrix} 0 \\ 0 \\ -P_c \end{pmatrix},$$

which gives  $\epsilon_1 = -s_{13}P_c$ ,  $\epsilon_3 = -s_{33}P_c$ , and the Poisson ratio  $\nu_{13} \equiv -\frac{\epsilon_1}{\epsilon_3} = -\frac{s_{13}}{s_{33}}$ .

In  $a$ -axis uniaxial loading with  $P_a$ , we have

$$\begin{pmatrix} \epsilon_1 \\ \epsilon_2 \\ \epsilon_3 \end{pmatrix} = \begin{pmatrix} s_{11} & s_{12} & s_{13} \\ s_{12} & s_{11} & s_{13} \\ s_{13} & s_{13} & s_{33} \end{pmatrix} \begin{pmatrix} -P_a \\ 0 \\ 0 \end{pmatrix},$$

which gives  $\epsilon_1 = -s_{11}P_a$ ,  $\epsilon_2 = -s_{12}P_a$ ,  $\epsilon_3 = -s_{13}P_a$ , and two Poisson ratios  $\nu_{31} \equiv -\frac{\epsilon_3}{\epsilon_1} = -\frac{s_{13}}{s_{11}}$  and  $\nu_{21} \equiv -\frac{\epsilon_2}{\epsilon_1} = -\frac{s_{12}}{s_{11}}$ .

Since we do not have elastic data from uniaxial compression, we have to make reasonable assumptions here. The first attempt is to assume the value for the Poisson ratio. Specifically for Hg1201, which does not have a huge  $a/c$  anisotropy, we assume  $\nu_{31}, \nu_{21}$  to be 0.2, a reasonable value for ceramics. Therefore,

$$\nu_{31} = -\frac{s_{13}}{s_{11}} = 0.2, \quad (\text{A3})$$

$$\nu_{21} = -\frac{s_{12}}{s_{11}} = 0.2. \quad (\text{A4})$$

With four unknowns  $s_{11}, s_{12}, s_{13}, s_{33}$ , and four equations (A1), (A2), (A3), and (A4), we obtain

$$\begin{aligned} s_{11} &= \frac{\kappa_a}{1 + \nu_{21} + \nu_{31}}, \\ s_{12} &= \frac{\nu_{21}\kappa_a}{1 + \nu_{21} + \nu_{31}}, \\ s_{13} &= \frac{\nu_{31}\kappa_a}{1 + \nu_{21} + \nu_{31}}, \\ s_{33} &= \kappa_c - \frac{2\nu_{31}\kappa_a}{1 + \nu_{21} + \nu_{31}}. \end{aligned}$$

## 2. Converting $dT_c/d\sigma$ to $dT_c/d\epsilon$

After the analysis of the previous section, we can express  $dT_c/dP_a$ ,  $dT_c/dP_c$ , and  $dT_c/dP$  in  $dT_c/d\epsilon_1$  and  $dT_c/d\epsilon_3$  by writing out the full derivatives of  $T_c$ :

$$\begin{aligned} \frac{dT_c}{dP_a} &= \frac{\partial T_c}{\partial \epsilon_1} \frac{\partial \epsilon_1}{\partial P_a} + \frac{\partial T_c}{\partial \epsilon_2} \frac{\partial \epsilon_2}{\partial P_a} + \frac{\partial T_c}{\partial \epsilon_3} \frac{\partial \epsilon_3}{\partial P_a} \\ &= (s_{11} + s_{12}) \frac{dT_c}{d\epsilon_1} + s_{13} \frac{dT_c}{d\epsilon_3}, \end{aligned}$$

$$\frac{dT_c}{dP_c} = 2 \frac{\partial T_c}{\partial \epsilon_1} \frac{\partial \epsilon_1}{\partial P_c} + \frac{\partial T_c}{\partial \epsilon_3} \frac{\partial \epsilon_3}{\partial P_c} = 2s_{13} \frac{dT_c}{d\epsilon_1} + s_{33} \frac{dT_c}{d\epsilon_3},$$

$$\begin{aligned} \frac{dT_c}{dP} &= 2 \frac{\partial T_c}{\partial \epsilon_1} \frac{\partial \epsilon_1}{\partial P} + \frac{\partial T_c}{\partial \epsilon_3} \frac{\partial \epsilon_3}{\partial P} \\ &= 2(s_{11} + s_{12} + s_{13}) \frac{dT_c}{d\epsilon_1} + (2s_{13} + s_{33}) \frac{dT_c}{d\epsilon_3}. \end{aligned}$$

The above three equations are not independent, abiding to the relationship  $dT_c/dP = 2dT_c/dP_a + dT_c/dP_c$ .

If we use the value of  $dT_c/dP_a$  and  $dT_c/dP$  from experiments and  $s_{11}, s_{12}, s_{13}, s_{33}$  from the above section, we will be able to solve the following linear equations:

$$\begin{pmatrix} s_{12} + s_{13} & s_{13} \\ 2(s_{11} + s_{12} + s_{13}) & 2s_{13} + s_{33} \end{pmatrix} \begin{pmatrix} dT_c/d\epsilon_1 \\ dT_c/d\epsilon_3 \end{pmatrix} = \begin{pmatrix} dT_c/dP_a \\ dT_c/dP \end{pmatrix}$$

TABLE II. Calculated compliance matrix elements; strain derivatives of  $T_c$  with different Poisson ratios.

$\nu_{21}, \nu_{31}$	0.15	0.2	Unit
$s_{11}$	$5.69 \times 10^{-3}$	$6.65 \times 10^{-3}$	/GPa
$s_{12}$	$-0.85 \times 10^{-3}$	$-1.33 \times 10^{-3}$	/GPa
$s_{13}$	$-0.85 \times 10^{-3}$	$-1.33 \times 10^{-3}$	/GPa
$s_{33}$	$7.84 \times 10^{-3}$	$8.79 \times 10^{-3}$	/GPa
$dT_c/d\epsilon_1$	-490	-435	K
$dT_c/d\epsilon_3$	352	278	K
$dT_c/da$	-126	-111.6	K/Å
$dT_c/dc$	36.8	29.1	K/Å

and obtain the values for

$$\frac{dT_c}{d\epsilon_1} \equiv \frac{dT_c}{da/a} = a \frac{dT_c}{da}, \quad \frac{dT_c}{d\epsilon_3} \equiv \frac{dT_c}{dc/c} = c \frac{dT_c}{dc}.$$

For Hg1201, we use the following parameters at ambient pressure:

$$\begin{aligned} dT_c/dP_c &= -3.6 \text{ K/GPa}, dT_c/dP = 1.75 \text{ K/GPa}, \\ \kappa_a &= 3.99 \times 10^{-3}/\text{GPa}, \kappa_c = 6.13 \times 10^{-3}/\text{GPa}, \\ a &= 3.8846 \text{ \AA}, c = 9.5486 \text{ \AA}. \end{aligned}$$

The calculated strain derivatives with different assumptions of Poisson's ratios are shown in Table II. It can be seen that the choice of Poisson's ratios would not affect the conclusion of this study. At higher pressures, the compressibilities  $\kappa_a, \kappa_c$  and lattice parameters  $a, c$  are different, and one needs to take them into account when calculating the  $dT_c/d\epsilon$  values at higher pressures. Poisson's ratio also changes with pressure [48], but at a much smaller scale at pressures below 20 GPa, and assuming them to be constant would be reasonable.

- 
- [1] A. Yamamoto, W.-Z. Hu, and S. Tajima, *Phys. Rev. B* **63**, 024504 (2000).
- [2] R. Liang, D. A. Bonn, and W. N. Hardy, *Phys. Rev. B* **73**, 180505(R) (2006).
- [3] L. Gao, Y. Y. Xue, F. Chen, Q. Xiong, R. L. Meng, D. Ramirez, C. W. Chu, J. H. Eggert, and H. K. Mao, *Phys. Rev. B* **50**, 4260 (1994).
- [4] A. Iyo, Y. Tanaka, H. Kito, Y. Kodama, P. M. Shirage, D. D. Shivagan, H. Matsuhata, K. Tokiwa, and T. Watanabe, *J. Phys. Soc. Jpn.* **76**, 094711 (2007).
- [5] B. Hunter, J. Jorgensen, J. Wagner, P. Radaelli, D. Hinks, H. Shaked, R. Hitterman, and R. V. Dreele, *Physica C* **221**, 1 (1994).
- [6] J. H. Eggert, J. Z. Hu, H. K. Mao, L. Beauvais, R. L. Meng, and C. W. Chu, *Phys. Rev. B* **49**, 15299 (1994).
- [7] F. Hardy, N. J. Hillier, C. Meingast, D. Colson, Y. Li, N. Barisic, G. Yu, X. Zhao, M. Greven, and J. S. Schilling, *Phys. Rev. Lett.* **105**, 167002 (2010).
- [8] J. S. Schilling, in *Handbook of High-Temperature Superconductivity: Theory and Experiment*, edited by J. R. Schrieffer and J. S. Brooks (Springer, New York, 2007), Chap. 11, p. 427.
- [9] A.-K. Klehe, A. Gangopadhyay, J. Diederichs, and J. Schilling, *Physica C* **213**, 266 (1993).
- [10] X. J. Chen, H. Q. Lin, and C. D. Gong, *Phys. Rev. Lett.* **85**, 2180 (2000).
- [11] X. Zhao, G. Yu, Y.-C. Cho, G. Chabot-Couture, N. Bari, P. Bourges, N. Kaneko, Y. Li, L. Lu, E. Motoyama, O. Vajk, and M. Greven, *Adv. Mater.* **18**, 3243 (2006).
- [12] N. Barišić, Y. Li, X. Zhao, Y. C. Cho, G. Chabot-Couture, G. Yu, and M. Greven, *Phys. Rev. B* **78**, 054518 (2008).
- [13] V. V. Struzhkin, Y. A. Timofeev, E. Gregoryanz, R. J. Hemley, and H.-k. Mao, [arXiv:cond-mat/0201520](https://arxiv.org/abs/cond-mat/0201520).
- [14] X. J. Chen, V. V. Struzhkin, R. J. Hemley, H. K. Mao, and C. Kendziora, *Phys. Rev. B* **70**, 214502 (2004).
- [15] X. J. Chen, V. V. Struzhkin, Y. Yu, A. F. Goncharov, C. T. Lin, H. K. Mao, and R. J. Hemley, *Nature (London)* **466**, 950 (2010).
- [16] M. Rivers, V. B. Prakapenka Vitali, A. Kubo, C. Pullins, C. Holl, and S. D. Jacobsen, *High Press. Res.* **28**, 273 (2008).
- [17] A. P. Hammersley, S. O. Svensson, M. Hanfland, A. N. Fitch, and D. Hausermann, *High Press. Res.* **14**, 235 (1996).
- [18] A. C. Larson and R. B. Von Dreele, Los Alamos National Laboratory Report, LAUR 86-748 (2000); B. H. Toby, *J. Appl. Crystallogr.* **34**, 210 (2001).
- [19] H. K. Mao, J. Xu, and P. M. Bell, *J. Geophys. Res.* **91**, 4673 (1986).
- [20] DAC was first warmed to 180 K and then pressure was immediately released, which was then measured at 90 K to be 1.9 GPa.
- [21] Y. Cao, Q. Xiong, Y. Y. Xue, and C. W. Chu, *Phys. Rev. B* **52**, 6854 (1995).
- [22] A. M. Balagurov, D. V. Sheptyakov, V. L. Aksenov, E. V. Antipov, S. N. Putilin, P. G. Radaelli, and M. Marezio, *Phys. Rev. B* **59**, 7209 (1999).
- [23] F. Birch, *Phys. Rev.* **71**, 809 (1947).
- [24] S. Sadewasser, J. S. Schilling, and A. M. Hermann, *Phys. Rev. B* **62**, 9155 (2000).
- [25] S. Sadewasser, J. S. Schilling, J. L. Wagner, O. Chmaissem, J. D. Jorgensen, D. G. Hinks, and B. Dabrowski, *Phys. Rev. B* **60**, 9827 (1999).
- [26] X. J. Chen, H. Q. Lin, W. G. Yin, C. D. Gong, and H. U. Habermeier, *Phys. Rev. B* **64**, 212501 (2001).
- [27] E. van Heumen, R. Lortz, A. B. Kuzmenko, F. Carbone, D. van der Marel, X. Zhao, G. Yu, Y. Cho, N. Barisic, M. Greven, C. C. Homes, and S. V. Dordevic, *Phys. Rev. B* **75**, 054522 (2007).
- [28] Note that  $-db/b \frac{da}{a} = 0.2$  means that when the  $a$  axis is compressed uniaxially, the tensile strain of the  $b$  axis is 20% the value of that of the  $a$  axis. This should not be confused with when uniaxially compressing the  $c$  axis  $\frac{db}{b} \frac{da}{a} = 1$ , which is required by tetragonal symmetry. Moreover, the result is insensitive to the choice of Poisson's ratio as long as it is between 0.15 and 0.3.
- [29] R. J. Cava, A. Santoro, D. W. Johnson, and W. W. Rhodes, *Phys. Rev. B* **35**, 6716 (1987).
- [30] J. M. Tarascon, L. H. Greene, W. R. Mckinnon, G. W. Hull, and T. H. Geballe, *Science* **235**, 1373 (1987).
- [31] Symmetry requires Hg1201 to have an average buckling angle of 180°. Reference [5] also confirms the 180° buckling angle up to 0.6 GPa. However, in the same study, they show that the buckling angle of the trilayer compound Hg1223 reduces from 178° at ambient pressure to 176.8° at 4 GPa, and 176.5° at 9.2 GPa, although the value at ambient pressure has an uncertainty of 0.5°.
- [32] N. Yamada and M. Ido, *Physica C* **203**, 240 (1992).
- [33] N. Mori, C. Murayama, H. Takahashi, H. Kaneko, K. Kawabata, Y. Iye, S. Uchida, H. Takagi, Y. Tokura, Y. Kubo, H. Sasakura, and K. Yamaya, *Physica C* **185–189**, 40 (1991).
- [34] H. Eisaki, N. Kaneko, D. L. Feng, A. Damascelli, P. K. Mang, K. M. Shen, Z.-X. Shen, and M. Greven, *Phys. Rev. B* **69**, 064512 (2004).

- [35] P. Blakeslee, R. J. Birgeneau, F. C. Chou, R. Christianson, M. A. Kastner, Y. S. Lee, and B. O. Wells, *Phys. Rev. B* **57**, 13915 (1998).
- [36] J. E. Schirber, W. R. Bayless, F. C. Chou, D. C. Johnston, P. C. Canfield, and Z. Fisk, *Phys. Rev. B* **48**, 6506 (1993).
- [37] H. Sakakibara, H. Usui, K. Kuroki, R. Arita, and H. Aoki, *Phys. Rev. Lett.* **105**, 057003 (2010).
- [38] H. Sakakibara, K. Suzuki, H. Usui, K. Kuroki, R. Arita, D. J. Scalapino, and H. Aoki, *Phys. Rev. B* **86**, 134520 (2012).
- [39] H. Sakakibara, H. Usui, K. Kuroki, R. Arita, and H. Aoki, *Phys. Rev. B* **85**, 064501 (2012).
- [40] W. Chen, G. Khaliullin, and O. P. Sushkov, *Phys. Rev. B* **83**, 064514 (2011).
- [41] S. Raghu, R. Thomale, and T. H. Geballe, *Phys. Rev. B* **86**, 094506 (2012).
- [42] S. J. L. Billinge and T. Egami, *Phys. Rev. B* **47**, 14386 (1993).
- [43] S. Agrestini, N. L. Saini, G. Bianconi, and A. Bianconi, *J. Phys. A* **36**, 9133 (2003).
- [44] P. M. Singer, A. W. Hunt, and T. Imai, *Phys. Rev. Lett.* **88**, 047602 (2002).
- [45] D. Rybicki *et al.*, *J. Supercond. Nov. Magn.* **22**, 179 (2009).
- [46] J. Jorgensen, *Proceedings of the Symposium on Superconductivity (ISS'99)* (Springer, New York, 2000).
- [47] I. P. R. Moreira, P. Rivero, and F. Illas, *J. Chem. Phys.* **134**, 074709 (2011).
- [48] C.-S. Zha, H.-k. Mao, and R. J. Hemley, *Proc. Natl. Acad. Sci. (USA)* **97**, 13494 (2000).